Unsteady electromagnetic radiative nanofluid stagnation-point flow from a stretching sheet with chemically reactive nanoparticles, Stefan blowing effect and entropy generation — Source link ↗

Puneet Rana, Nisha Shukla, O. Anwar Bég, Ali Kadir ...+1 more authors

Institutions: Jaypee Institute of Information Technology, University of Salford

Related papers:

- Stefan Blowing Impacts on Unsteady MHD Flow of Nanofluid over a Stretching Sheet with Electric Field, Thermal Radiation and Activation Energy

- The Combined Magneto Hydrodynamic and Electric Field Effect on an Unsteady Maxwell Nanofluid Flow over a Stretching Surface under the Influence of Variable Heat and Thermal Radiation

- Unsteady MHD slip flow of non Newtonian power-law nanofluid over a moving surface with temperature dependent thermal conductivity

- Chemical Reaction and Uniform Heat Generation or Absorption Effects on MHD Stagnation-Point Flow of a Nanofluid over a Porous Sheet

- Numerical study of entropy analysis for electrical unsteady natural magnetohydrodynamic flow of nanofluid and heat transfer

Unsteady electromagnetic radiative nanofluid stagnation-point flow from a stretching sheet with chemically reactive nanoparticles, Stefan blowing effect and entropy generation

Rana, P, Shukla, N, Beg, OA, Kadir, A and Singh, B

http://dx.doi.org/10.1177/2397791418782030

Title	Unsteady electromagnetic radiative nanofluid stagnation-point flow from a stretching sheet with chemically reactive nanoparticles, Stefan blowing effect and entropy generation
Authors	Rana, P, Shukla, N, Beg, OA, Kadir, A and Singh, B
Publication title	Proceedings of the Institution of Mechanical Engineers, Part N: Journal of Nanomaterials, Nanoengineering and Nanosystems
Publisher	SAGE
Type	Article
USIR URL	This version is available at: http://usir.salford.ac.uk/id/eprint/45170/
Published Date	2018

UNSTEADY ELECTROMAGNETIC RADIATIVE NANOFLUID STAGNATION-POINT FLOW FROM A STRETCHING SHEET WITH CHEMICALLY REACTIVE NANOPARTICLES, STEFAN BLOWING EFFECT AND ENTROPY GENERATION

Puneet Rana[1*], Nisha Shukla[1], O. Anwar Bég[2], A. Kadir [3] and Bani Singh[1]

*[1]Department of Mathematics, Jaypee Institute of Information Technology,
A-10, Sector-62, Noida-201307, Uttar Pradesh, **India.***
*[2]Fluid Mechanics, Propulsion and Nanosystems, Aeronautical and Mechanical Engineering, School of Computing, Science & Engineering, University of Salford, Newton Building, M54WT, **UK.***
*[3]Corrosion and Materials, Aeronautical and Mechanical Engineering, School of Computing, Science & Engineering, University of Salford, Newton Building, M54WT, **UK.***

Abstract: *The present article investigates the combined influence of nonlinear radiation, Stefan blowing and chemical reactions on unsteady EMHD stagnation point flow of a nanofluid from a horizontal stretching sheet. Both electrical and magnetic body forces are considered. In addition, the effects of velocity slip, thermal slip and mass slip are considered at the boundaries. An analytical method named as homotopy analysis method is applied to solve the non-dimensional system of nonlinear partial differential equations which are obtained by applying similarity transformations on governing equations. The effects of emerging parameters including Stefan blowing parameter, electric parameter, magnetic parameter etc. on the important physical quantities are presented graphically. Additionally, an entropy generation analysis is provided in this article for thermal optimization. The flow is observed to be accelerated both with increasing magnetic field and electrical field. Entropy generation number is markedly enhanced with greater magnetic field, electrical field and Reynolds number, whereas it is reduced with increasing chemical reaction parameter.*

Keywords: *Stefan blowing; Nonlinear radiation; Nanofluid; EMHD; Entropy; Chemical reaction; Electrical field; Magnetic field; Homotopy solutions; Unsteady flow.*

Nomenclature

B_0	Magnetic Field Strength (T)	Nb	Brownian Motion Parameter (--)
C	Nanoparticles Concentration (--)	Nt	Thermophoresis Parameter (--)
D_B	Brownian Diffusion (m^2/s)	Pr	Prandtl number (--)
D_T	Thermophoresis Diffusion (m^2/s)	q	Embedding Parameter (--)
E	Electric Parameter (--)	R	Radiation Parameter (--)
E_0	Electric Field Strength (N/C)	Re	Reynolds Number (--)
Ec	Eckert Number (--)	s	Stefan Blowing Parameter (--)
G	Dimensionless Stream function (--)	S	Dimensionless Concentration(--)
k	Thermal Conductivity (W/m-K)	Sc	Schmidt Number (--)
K	Chemical Reaction Parameter (--)	t	Time(s)
M	Magnetic Parameter (--)	$t_r = \dfrac{T_w}{T_\infty}$	Temperature Ratio (--)
N_1	Velocity Slip Parameter (--)	$\bar{u}$	Velocity (m/s) along $\bar{x}$-axis
N_2	Thermal Slip Parameter (--)	$\bar{v}$	Velocity (m/s) along $\bar{y}$-axis
N_3	Mass Slip Parameter (--)	x, y	Similarity Variables (--)

Greek Symbols

α	Thermal Diffusivity (m^2/s)	Ω	Dimensionless Temperature Difference
β	Stagnation Parameter (--)	(ρc)	Heat Capacity (J/Km^3)

μ	Dynamic Viscosity (Ns/m^2)	θ	Dimensionless Temperature (--)
σ	Electrical Conductivity (S/m)	χ	Diffusive Constant (--)
ψ	Stream Function (m^2/s)	λ_1	Dimensionless Velocity slip parameter
υ	Kinematic Viscosity (m^2/s)	λ_2	Dimensionless Thermal slip parameter
τ	Non-Dimensional Time (--)	λ_3	Dimensionless Mass slip parameter
τ_1	Ratio of Heat Capacities (--)		

Subscripts

∞	Ambient condition	nf	Nanofluid
w	Condition on surface	p	Nanoparticles

1. INTRODUCTION

Stefan blowing (wall injection) finds substantial applications in industrial systems such as drying and purifying processes where boundaries are perforated. The "blowing effect" occurs due to the mass transfer of molecules or nanoparticles from one location to another. Mass transfer is also fundamental to absorption, evaporation, combustion, distillation and materials synthesis. The concept of blowing effect is provided by the Stefan problem which is an application of mass transfer [1] of species. Stefan blowing problem states that there exist a relation between the rate of mass transfer and flow field at the wall, because mass transfer is dependent upon the flow field and flow field is generated by mass blowing at wall. Fang and Jing [2] have considered the Stefan blowing effects to investigate the mass and heat transfer of a viscous fluid over a linearly stretching sheet and observed that velocity, temperature and concentration are increasing

functions of blowing parameter. Uddin *et al.* [3] have provided a numerical study of bioconvection nanofluid flow over a plate incorporating the effects of Stefan blowing, velocity, thermal and mass slips at the wall. In addition, Uddin *et al.* [4] investigated the second order velocity slip and Stefan blowing effects for bio-nanofluid flow with passively boundary conditions.

Nanofluids [5–8] constitute based fluids containing nano-sized metallic particles. The presence of metallic nano-particles enhances thermal conductivity properties of such fluids. Shahzad *et al.* [9] have presented the analytical study of the magnetohydrodynamic flow of Cu based nanoparticles. They have observed that the heat transfer enhances near the surface due to the presence of Cu-nanoparticles. Sheikholeslami and Bhatti [10] have applied finite element method to investigate the influence of Coulomb force on the force convective nanofluid flow .and observed an enhancement in Nusselt number due to electric field. A broad literature is available regarding the different types of study on nanofluid [11–18] due to a vast amount of applications of it in industries and engineering field.

In high-temperature materials processing, thermal radiation is significant. Generally two modelling approaches are employed for simulating radiative heat transfer effects, namely linear and nonlinear models. Nonlinear radiation is valid for both high and low temperature difference but linear radiation is valid only for low temperature difference. Thus, to provide a more general and physically realistic simulation, in the present work, we consider the nonlinear thermal radiation in the present article. Numerous studies of radiative flows have been communicated. Khan *et al.* [19] have investigated the nonlinear radiation effect on a magnetohydrodynamic nanofluid flow from a sheet and have shown that the rate of heat transfer is increased for a shrinking sheet whereas it is decreased for a stretching sheet. Bhatti and Rashidi [20] have

examined the combined influence of thermal radiation and diffusion on nanofluid flow over a stretching sheet. Sheikholeslami [21] has investigated the effect of Lorentz force and radiation on a $Fe_3O_4 - H_2O$ nanofluid and achieved and enhancement in rate of heat transfer due to an enhancement in radiation parameter. Rashidi *et al.* [22] have considered the impact of thermal radiation with aligned magnetic field on a Cu and Al_2O_3-water nanofluid flow over a stretching sheet. Further studies include [23,24] for different configurations and with multiple body force effects.

Materials processing systems often involve chemical reactions, which may be *destructive* or *constructive* in nature and can influence significantly heat and mass diffusion phenomena. Generally boundary layer flow models utilize first order chemical reaction effects and assume the reaction to be destructive. Chemical reactions are instrumental in transforming material constitution. This phenomenon also arises in chemical engineering industries, electrochemistry, hydrolysis, electro-plating and combustion processes (furnaces, fires, jet propulsion etc). Interesting studies of reactive flows include Mishra *et al.* [25] on magnetic viscoelastic fluids, Mohamed [26] on two-phase nanofluids, Venkateswarlu and Narayana [27] on radiative rotating nanofluid flows, Bég *et al.*[28] on dissipative radiative hydromagnetic double diffusion transport and Matin and Pop [29] on porous nanofluid flows. Further investigations include [30–33] in which chemical reaction has been shown to have a significant influence on heat and/or mass transfer characteristics.

The second law of thermodynamics provides a way to quantify the level of disorder of a thermodynamically system. This study is known as *entropy generation analysis* which is very useful in optimizing thermal engineering systems to operate at high working efficiency. The

method of entropy generation minimization was originally proposed by Bejan [34] in 1996. Many researchers have investigated the effects of physical parameters on entropy generation in various thermal flow regimes. Tshehla and Makinde [35] have calculated the rate of entropy generation in steady flow of a liquid with variable viscosity for two concentric cylindrical pipes. Das *et al.*[36] have elaborated on entropy generation in an unsteady MHD flow of nanofluid from a stretching sheet, observing that metallic nanoparticles generate a large amount of entropy. Rehman *et al.* [37] have considered the steady Jeffery nanofluid flow over a stretching sheet, indicating that entropy generation number is an increasing function of thermophoresis parameter, Eckert number and Brinkman number. Qing *et al.* [38] have studied the entropy generation analysis on a magnetohydrodynamic flow of Casson nanofluid with the effects of chemical reactions and nonlinear thermal radiation over a stretching surface. Bhatti *et al.* [39] have applied successive linearization method to investigate the entropy generation analysis for non-Newtonian nanofluid over stretching surface.

The preceding studies have not considered entropy generation for the combined unsteady electro-magnetic nanofluid stagnation flow from a stretching sheet with the simultaneous effects of Stefan blowing, chemical reaction, nonlinear thermal radiation, velocity slip, thermal slip and mass slip. Both electrical and magnetic body forces are incorporated in the mathematical model [40]. The system of governing equations has been transformed into a non-dimensional system of nonlinear partial differential equations by applying similarity transformations. The non-dimensional boundary value problem is thereafter solved with the homotopy analysis method (HAM) employing power-series expansions. Homotopy analysis method is discovered by Liao[41–43] which is an excellent analytical technique to solve the nonlinear ordinary and partial differential equations. Rehman *et al.* [44] have compared the numerical results obtained via

shooting technique with HAM results of Casson fluid flow over an exponentially stretching sheet. In this article, we employ this technique to solve the system of nonlinear partial differential equations [45] which a non-dimensional form of governing equations. The present problem has applications in thermal management [46] of high heat flux electronics such as heat pipes, energy conversion devices and biomedical research.

The article is structured as follows. Section 1 is the introductory part. Section 2 covers the problem formulation. Section 3 entails the entropy generation analysis. Section 4 elaborates the analytical homotopy solutions and convergence characteristics. A brief discussion of results is presented in section 5. Section 6 summarizes the conclusions. The current work is relevant to electromagnetic nano-materials processing.

2. MATHEMATICAL MODEL

In this problem, we analyze the composite influence of Stefan blowing, destructive first order chemical reaction and nonlinear radiation on two-dimensional time dependent EMHD (Electro-magneto-hydrodynamic) stagnation point flow[47] of an electrically-conducting incompressible nanofluid from a stretching sheet. **Fig.1** represents the geometry of the problem in which the point O is a stagnation point. The horizontal $\bar{x}$ -axis is located along the sheet and the vertical $\bar{y}$ -axis is fixed in a direction perpendicular to the sheet. At the surface of sheet, the effects of velocity, thermal and mass slips are also considered. Such phenomena are known to arise in materials processing systems. Under these considerations, the boundary layer equations for conservation of mass, momentum, energy and nanoparticle (species) concentrations are defined may be shown to assume the form [21,48,49]:

$$\frac{\partial \bar{u}}{\partial \bar{x}} + \frac{\partial \bar{v}}{\partial \bar{y}} = 0, \tag{1}$$

$$\frac{\partial \bar{u}}{\partial t} + \bar{u}\frac{\partial \bar{u}}{\partial \bar{x}} + \bar{v}\frac{\partial \bar{u}}{\partial \bar{y}} = \frac{\partial \bar{u}_\infty}{\partial t} + \bar{u}_\infty \frac{d\bar{u}_\infty}{d\bar{x}} + \upsilon_{nf}\frac{\partial^2 \bar{u}}{\partial \bar{y}^2} - \frac{\sigma_{nf}B_0^2}{\rho_{nf}}(\bar{u} - \bar{u}_\infty) + \sigma_{nf}\frac{E_0 B_0}{\rho_{nf}}, \tag{2}$$

$$\frac{\partial T}{\partial t} + \bar{u}\frac{\partial T}{\partial \bar{x}} + \bar{v}\frac{\partial T}{\partial \bar{y}} = \alpha_{nf}\frac{\partial^2 T}{\partial \bar{y}^2} + \frac{\mu_{nf}}{(\rho c)_{nf}}\left(\frac{\partial \bar{u}}{\partial \bar{y}}\right)^2 + \tau_1\left[D_B\frac{\partial C}{\partial \bar{y}}\frac{\partial T}{\partial \bar{y}} + \frac{D_T}{T_\infty}\left(\frac{\partial T}{\partial \bar{y}}\right)^2\right] - \frac{1}{(\rho c)_{nf}}\frac{\partial q_r}{\partial \bar{y}}, \tag{3}$$

$$\frac{\partial C}{\partial t} + \bar{u}\frac{\partial C}{\partial \bar{x}} + \bar{v}\frac{\partial C}{\partial \bar{y}} = D_B\frac{\partial^2 C}{\partial \bar{y}^2} + \frac{D_T}{T_\infty}\frac{\partial^2 T}{\partial \bar{y}^2} - K(C - C_\infty), \tag{4}$$

The following boundary conditions are imposed at the sheet (wall) and in the free stream[3] :

$$\text{at } \bar{y} = 0, \quad \bar{u} = \bar{u}_w(\bar{x}) + N_1\frac{\partial \bar{u}}{\partial \bar{y}}, \quad \bar{v} = -\frac{D_B}{1 - C_w}\left(\frac{\partial C}{\partial \bar{y}}\right), \quad T = T_w + N_2\frac{\partial T}{\partial \bar{y}}, \quad C = C_w + N_3\frac{\partial C}{\partial \bar{y}},$$

$$\text{as } \bar{y} \to \infty, \quad \bar{u} \to \bar{u}_\infty, \quad T = T_\infty, \quad C = C_\infty, \tag{5}$$

where $\bar{u}$ (m/sec), $\bar{v}$ (m/sec) are the velocities along the $\bar{x}$ (m) and $\bar{y}$ (m) axes respectively and t (s) represents the time. The velocity of the sheet is $\bar{u}_w(x) = b\bar{x}$ where b is the sheet (wall) stretching parameter and free stream velocity is defined as $\bar{u}_\infty = a\bar{x}$. The term υ_{nf} (m²/s) represents the kinematic viscosity whereas μ_{nf} (Ns/m²) represents the dynamic viscosity of nanofluid. In addition, the term ρ_{nf} (kg/m³) is density of nanofluid, σ_{nf} (S/m) is electrical conductivity of nanofluid, k_{nf} is thermal conductivity of nanofluid, $(\rho c)_{nf}$ (J/K-m³) is heat capacity of nanofluid and α_{nf} (m²/s) $= \dfrac{k_{nf}}{(\rho c)_{nf}}$ is thermal diffusivity of nanofluid . B_0 (T) and

E_0 (N/C) define magnetic and electric field strength respectively. The terms D_B (m² /s) and

D_T (m² /s) signify Brownian and thermophoresis diffusion respectively and K (s⁻¹) represents

chemical reaction coefficient. T (K) and T_∞ (K) are nanofluid and ambient temperatures, C and

C_∞ are nanoparticles volume fraction and ambient volume fraction and the term

$\tau_1 = \dfrac{(\rho c)_p}{(\rho c)_{nf}}$ represents the ratio of heat capacities (J/K-m³) of nanoparticles to nanofluid

whereas N_1, N_2 and N_3 are velocity slip, thermal slip and mass slip parameters respectively.

T_w and C_w are respectively nanofluid temperature and nanoparticles volume fraction at surface.

The radiative heat flux q_r (W/m²) is defined as[50]:

$$q_r = -\frac{4 \times \text{Stefan-Boltzmann constant } (\sigma_1)}{3 \times \text{Rosseland mean absorption coefficient } (k_1)} \frac{\partial T^4}{\partial y}, \tag{6}$$

which is obtained by Rosseland approximations. This approximation is valid for optically-thick

fluids which can absorb or emit radiation at their boundaries.

Proceeding with the analysis, the following similarity transformations are applied to convert

Eqns. (1)-(5) into non-dimensional form [51,52]:

$$x = \sqrt{\frac{a}{\upsilon_{nf} y}} \, \overline{y}, \quad \psi = \sqrt{a\upsilon_{nf} y} \, \overline{x} \, G(x, y), \quad \overline{u} = a \, \overline{x} \, \frac{\partial G(x, y)}{\partial x}, \quad \overline{v} = -\sqrt{a\upsilon_{nf} y} G(x, y),$$

$$\theta(x, y) = \frac{T - T_\infty}{T_w - T_\infty}, \quad S(x, y) = \frac{C - C_\infty}{C_w - C_\infty}, \quad y = 1 - e^{-\tau}, \quad \tau = at, \tag{7}$$

where x is similarity variable, $G(x, y)$, $\theta(x, y)$ and $S(x, y)$ are non-dimensional stream function,

temperature and nanoparticles concentration, respectively and τ represents the non-dimensional

time. The term ψ represents the dimensional stream function which satisfies Eqn. (1) and is

defined by the Cauchy-Riemann equations, $\bar{u} = \dfrac{\partial \psi}{\partial \bar{y}}, \ \bar{v} = -\dfrac{\partial \psi}{\partial \bar{x}}.$

The non-dimensional forms of Eqns. (2)-(5) can be written as:

$$\frac{\partial^3 G}{\partial x^3} + y\left(1 - \left(\frac{\partial G}{\partial x}\right)^2 + G\frac{\partial^2 G}{\partial x^2}\right) - \frac{x}{2}(y-1)\frac{\partial^2 G}{\partial x^2} + y(y-1)\frac{\partial^2 G}{\partial y \partial x} - M^2 y\left(\frac{\partial G}{\partial x} - 1 - E\right) = 0, \tag{8}$$

$$\frac{1}{\Pr}\left(\frac{\partial^2 \theta}{\partial x^2} + Nb\frac{\partial \theta}{\partial x}\frac{\partial S}{\partial x} + Nt\left(\frac{\partial \theta}{\partial x}\right)^2\right) + y(y-1)\frac{\partial \theta}{\partial y} - \frac{x}{2}(y-1)\frac{\partial \theta}{\partial x} + yG\frac{\partial \theta}{\partial x} + Ec\left(\frac{\partial^2 G}{\partial x^2}\right)^2$$

$$+\frac{4}{3\Pr}R\left[\begin{array}{l}\dfrac{\partial^2 \theta}{\partial x^2} + (t_r - 1)^3\left(3\theta^2\left(\dfrac{\partial \theta}{\partial x}\right)^2 + \theta^3\dfrac{\partial^2 \theta}{\partial x^2}\right) + 3(t_r - 1)\left(\theta\dfrac{\partial^2 \theta}{\partial x^2} + \left(\dfrac{\partial \theta}{\partial x}\right)^2\right) \\[4mm] +3(t_r - 1)^2\left(\dfrac{\partial^2 \theta}{\partial x^2}\theta^2 + 2\theta\left(\dfrac{\partial \theta}{\partial x}\right)^2\right)\end{array}\right] = 0, \tag{9}$$

$$\frac{\partial^2 S}{\partial x^2} + \frac{Nt}{Nb}\frac{\partial^2 \theta}{\partial x^2} + Sc\left[yG\frac{\partial S}{\partial x} + y(y-1)\frac{\partial S}{\partial y} - \frac{x}{2}(y-1)\frac{\partial S}{\partial x}\right] - y\omega S = 0, \tag{10}$$

at $x = 0$, $\ G(0, y) = \dfrac{s}{Sc}\dfrac{\partial S(0, y)}{\partial x}, \quad \dfrac{\partial G(0, y)}{\partial x} = \beta + \lambda_1\dfrac{\partial^2 G(0, y)}{\partial x^2},$

$$\theta(0, y) = 1 + \lambda_2\frac{\partial \theta(0, y)}{\partial x}, \ S(0, y) = 1 + \lambda_3\frac{\partial S(0, y)}{\partial x},$$

as $x \to \infty$, $\ \dfrac{\partial G(x, y)}{\partial x} = 1, \quad \theta(x, y) = 0, \quad S(x, y) = 0,$ \hfill (11)

where the non-dimensional physical parameters are defined as:

$M = \sqrt{\dfrac{\sigma_{nf} B_0^2}{a \rho_{nf}}}$ is magnetic parameter, $E = \dfrac{E_0}{B_0 \bar{u}_\infty}$ is electric field parameter, $\Pr = \dfrac{\upsilon_{nf} (\rho c)_{nf}}{k_{nf}}$ is

Prandtl number, $Nb = \dfrac{\tau_1 D_B (C_w - C_\infty)}{\alpha_{nf}}$ is Brownian motion parameter, $Nt = \dfrac{\tau_1 D_T (T_w - T_\infty)}{T_\infty \alpha_{nf}}$ is

thermophoresis parameter, $Ec = \dfrac{\bar{u}_w^2}{c_{nf} (T_w - T_\infty)}$ is local Eckert number, $Sc = \dfrac{\upsilon_{nf}}{D_B}$ is Schmidt

number, $R = \dfrac{4 \sigma_1 T_\infty^3}{k_{nf} k_1}$ is radiation parameter, $t_r = \dfrac{T_w}{T_\infty}$ is temperature ratio, $\mathrm{Re} = \dfrac{a \bar{x}^2}{\upsilon_{nf}}$ is local

Reynolds number, $\omega = \dfrac{K}{a}$ is chemical reaction parameter, $s = \dfrac{(C_w - C_\infty)}{(1 - C_w) y}$ is Stefan blowing

parameter, $\lambda_1 = N_1 \sqrt{\dfrac{a}{\upsilon_{nf} y}}$ is velocity slip parameter , $\lambda_2 = N_2 \sqrt{\dfrac{a}{\upsilon_{nf} y}}$ is thermal slip parameter,

$\lambda_3 = N_3 \sqrt{\dfrac{a}{\upsilon_{nf} y}}$ is mass slip parameter and β is the stagnation parameter.

In this study, the important engineering quantities are the skin friction coefficient, the local

Nusselt number and Sherwood number. These quantities evaluate the transport phenomena at the

wall (sheet) and are defined respectively as:

Skin friction coefficient:

$$C_{nf} = \dfrac{\tau_w}{\rho_{nf} (a \bar{x})^2}, \tag{12}$$

where τ_w represents wall stress, which is defined as:

$$\tau_w = \mu_{nf} \dfrac{\partial \bar{u}}{\partial \bar{y}} \bigg|_{\bar{y}=0}. \tag{13}$$

Using eqs. (7), (12) and (13), we obtain

$$Cf = \sqrt{\frac{y}{\text{Re}}} C_{nf} = G''(0, y).$$

(14)

Local Nusselt number[19,21,53]:

$$Nu = \frac{\overline{x}}{k_{nf}(T_w - T_\infty)}(q_w + q_r)_{\overline{y}=0},$$

(15)

where q_w represents heat flux at wall and is defined as:

$$q_w = \left(-k_{nf}\nabla T + h_p j_p\right)_{\overline{y}=0},$$

(16)

Here $h_p = c_p(T_w - T_\infty)$ is enthalpy and j_p is the sum of the Brownian and thermophoresis diffusion terms, defined as.

$$j_p = -\rho_p\left(D_B\nabla C + D_T\frac{\nabla T}{T}\right).$$

(17)

Using eqs. (6), (7), (15), (16) and (17), we obtain

$$Nur = \sqrt{\frac{y}{\text{Re}}} Nu = -\left[\theta'(0, y)\left(1 + Nt + \frac{4R}{3}t_r^3\right) + NbS'(0, y)\right].$$

(18)

Sherwood Number:

$$Sh = \frac{q_m\overline{x}}{D_B C_\infty},$$

(19)

where q_m represents mass flux at wall and defined as: $q_m = \frac{j_p}{\rho_p}$.

(20)

Using Eqns. (6), (17), (19) and (20), we obtain

$$Shr = \sqrt{\frac{y}{\text{Re}}} Sh = -\left[S'(0, y) + \frac{Nt}{Nb} \theta'(0, y) \right].$$
(21)

3. ENTROPY GENERATION ANALYSIS

The volumetric rate of entropy generation, due to the effects of heat transfer, nonlinear radiation, viscous dissipation, diffusion and electromagnetic field is defined as [36,54]:

$$S_G = \frac{k_{nf}}{T_\infty^2} \left[1 + \frac{16\sigma_1}{3k_{nf}k_1} \right] \left(\frac{\partial T}{\partial y} \right)^2 + \frac{\mu_{nf}}{T_\infty} \left(\frac{\partial \bar{u}}{\partial y} \right)^2 + \frac{R_g D_B}{C_\infty} \left(\frac{\partial C}{\partial y} \right)^2$$
$$+ \frac{R_g D_B}{T_\infty} \left(\frac{\partial C}{\partial y} \right) \left(\frac{\partial T}{\partial y} \right) + \frac{\sigma_{nf} B_0^2}{T_\infty} (\bar{u}_\infty - \bar{u})^2 + \frac{\sigma_{nf} E_0 B_0 \bar{u}}{T_\infty},$$
(22)

where R_g (J mol^{-1}K^{-1}) is gas constant.

The characteristic rate of entropy generation is: $S_c = \frac{k_{nf}(T_w - T_\infty)^2}{\bar{x}^2 T_\infty^2}.$
(23)

The non-dimensional entropy generation number is obtained by applying similarity transformations on the ratio of S_G and S_C which is defined as:

$$Ns = \frac{S_G}{S_c} = \frac{\text{Re}}{y} \left[\left(1 + \frac{4R}{3} \right) \left(\frac{\partial \theta}{\partial x} \right)^2 + \frac{\text{Pr}.Ec}{\Omega} \left\{ \left(\frac{\partial^2 G}{\partial x^2} \right)^2 + yM^2 \left[\left(1 - \frac{\partial G}{\partial x} \right)^2 + E \frac{\partial G}{\partial x} \right] \right\} + \frac{\chi}{\Omega} \left(\frac{1}{\Omega} \left(\frac{\partial S}{\partial x} \right)^2 + \frac{\partial \theta}{\partial x} \frac{\partial S}{\partial x} \right) \right],$$
(24)

where $\chi = \frac{R_g D C_\infty}{k_{nf}}$ is diffusive constant and $\Omega = \frac{T_w - T_\infty}{T_\infty}$ is non-dimensional temperature difference.

4. SOLUTIONS WITH HOMOTOPY ANALYSIS METHOD (HAM)

To solve the non-dimensional system of nonlinear partial differential Eqns. (7)-(9) with boundary conditions (10), the homotopy analysis method has been applied. On the basis of suggestions of Liao[42], we have selected the following initial guesses, linear operators and auxiliary functions:

The *initial guesses*:

$$G_0(x,y) = \frac{\beta-1}{1+\lambda_1}\left(1-e^{-x}\right) - \frac{s}{Sc(1+\lambda_3)} + x, \quad \theta_0(x,y) = \frac{e^{-x}}{1+\lambda_2}, \quad S_0(x,y) = \frac{e^{-x}}{1+\lambda_3}, \tag{25}$$

which are satisfied the boundary conditions (10).

The *linear operators*:

$$L_G(G) = \frac{\partial^3 G}{\partial x^3} - \frac{\partial G}{\partial x}, \quad L_\theta(\theta) = \frac{\partial^2 \theta}{\partial x^2} + \frac{\partial \theta}{\partial x}, \quad L_S(S) = \frac{\partial^2 S}{\partial x^2} + \frac{\partial S}{\partial x}, \tag{26}$$

which are satisfied the conditions:

$$L_G(C_1 + C_2 e^x + C_3 e^{-x}) = 0, \quad L_\theta(C_4 + C_5 e^{-x}) = 0, \quad L_S(C_6 + C_7 e^{-x}) = 0. \tag{27}$$

The auxiliary functions: $H_G = 1, H_\theta = 1, H_S = 1$.

The zero$^{\text{th}}$ order equation:

$$(1-q)L_G[\xi_G(x,y,q) - G_0(x,y)] = qh_G H_G(x,y)N_G[\xi_G(x,y,q), \xi_\theta(x,y,q), \xi_S(x,y,q)], \tag{28}$$

$$(1-q)L_\theta[\xi_\theta(x,y,q) - \theta_0(x,y)] = qh_\theta H_\theta(x,y)N_\theta[\xi_\theta(x,y,q), \xi_\theta(x,y,q), \xi_S(x,y,q)], \tag{29}$$

$$(1-q)L_S[\xi_S(x,y,q)-S_0(x,y)]=qh_SH_S(x,y)N_S[\xi_S(x,y,q),\xi_\theta(x,y,q),\xi_S(x,y,q)],\qquad(30)$$

associated with: $\xi_G(0,y)-\dfrac{s}{Sc}\dfrac{\partial\xi_S(0,y)}{\partial x}=0,\quad \dfrac{\partial\xi_G(0,y)}{\partial x}-\beta-\lambda_1\dfrac{\partial^2\xi_G(0,y)}{\partial x^2}=0,$

$$\xi_\theta(0,y)-\lambda_2\frac{\partial\xi_\theta(0,y)}{\partial x}-1=0,\ \xi_S(0,y)-\lambda_3\frac{\partial\xi_S(0,y)}{\partial x}-1=0,$$

as $x\to\infty,\qquad \dfrac{\partial\xi_G(x,y)}{\partial x}=1,\ \xi_\theta(x,y)=0,\quad \xi_S(x,y)=0.\qquad(31)$

where $q\in[0,1]$ and h_G, h_θ and h_S are the auxiliary parameters. The convergence of Eqns. (28)-(31) are dependent on the values of these auxiliary parameters. The term N_G, N_θ and N_S are defined as:

$$N_G=\frac{\partial^3\xi_G}{\partial x^3}+y\left(1-\left(\frac{\partial\xi_G}{\partial x}\right)^2+\xi_G\frac{\partial^2\xi_G}{\partial x^2}\right)+y(y-1)\frac{\partial^2\xi_G}{\partial y\partial x}-\frac{x}{2}(y-1)\frac{\partial^2\xi_G}{\partial x^2}-M^2y\left(\frac{\partial\xi_G}{\partial x}-1-E\right),$$

$$(32)$$

$$N_\theta=\frac{1}{Pr}\left(\frac{\partial^2\xi_\theta}{\partial x^2}+Nb\frac{\partial\xi_\theta}{\partial x}\frac{\partial\xi_S}{\partial x}+Nt\left(\frac{\partial\xi_\theta}{\partial x}\right)^2\right)+y(y-1)\frac{\partial\xi_\theta}{\partial y}-\frac{x}{2}(y-1)\frac{\partial\xi_\theta}{\partial x}+y\xi_G\frac{\partial\xi_\theta}{\partial x}+Ec\left(\frac{\partial^2\xi_G}{\partial x^2}\right)^2$$

$$+\frac{4R}{3Pr}\left[\frac{\partial^2\xi_\theta}{\partial x^2}+(t_r-1)^3\left(3\xi_\theta^2\left(\frac{\partial\xi_\theta}{\partial x}\right)^2+\xi_\theta^3\frac{\partial^2\xi_\theta}{\partial x^2}\right)+3(t_r-1)\left(\xi_\theta\frac{\partial^2\xi_\theta}{\partial x^2}+\left(\frac{\partial\xi_\theta}{\partial x}\right)^2\right)\right.$$

$$+3(t_r-1)^2\left(\frac{\partial^2\xi_\theta}{\partial x^2}\xi_\theta^2+2\xi_\theta\left(\frac{\partial\xi_\theta}{\partial x}\right)^2\right)\right],\qquad(33)$$

$$N_S=\frac{\partial^2\xi_S}{\partial x^2}+\frac{Nt}{Nb}\frac{\partial^2\xi_\theta}{\partial x^2}+Sc\left[y\xi_G\frac{\partial\xi_S}{\partial x}+y(y-1)\frac{\partial\xi_S}{\partial y}-\frac{x}{2}(y-1)\frac{\partial\xi_S}{\partial x}\right]-y\omega\xi_S.\qquad(34)$$

On differentiating Eqns. (28)-(30) m times and dividing by $m!$, then with subsequent substitution of $q = 0$, we obtain:

$$L_G(G_m(x, y) - \chi_{m-1}G_{m-1}(x, y)) = h_G H_G R_m^G(x, y),$$ (35)

$$L_\theta(\theta_m(x, y) - \chi_{m-1}\theta_{m-1}(x, y)) = h_\theta H_\theta R_m^\theta(x, y),$$ (36)

$$L_S(S_m(x, y) - \chi_{m-1}S_{m-1}(x, y)) = h_S H_S R_m^S(x, y),$$ (37)

with boundary conditions:

at

$$x = 0, \ G_m(x, y) - \frac{s}{Sc}\frac{\partial S_m(x, y)}{\partial x} = 0, \ \frac{\partial G_m(x, y)}{\partial x} - \lambda_1 \frac{\partial^2 G_m(x, y)}{\partial x^2} = 0, \ \theta_m(x, y) - \lambda_2 \frac{\partial \theta_m(x, y)}{\partial x} = 0,$$

$$S_m(x, y) - \lambda_3 \frac{\partial S_m(x, y)}{\partial x} = 0,$$

as $x \to \infty, G_m(x, y) = 0, \ \theta_m(x, y) = 0$ and $S_m(x, y) = 0$. (38)

In the above Eqns., the term $R_m^G(x, y)$, $R_m^\theta(x, y)$ and $R_m^S(x, y)$ are defined as:

$$R_m^G(x, y) = \frac{1}{m-1!}\frac{\partial^{m-1}N_G}{\partial q^{m-1}}\bigg|_{q=0} = \frac{\partial^3 G_{m-1}}{\partial x^3} + y\left(\sum_{i=0}^{m-1}\left(G_{m-1}\frac{\partial^2 G_{m-i-1}}{\partial x^2} - \left(\frac{\partial G_{m-1}}{\partial x}\right)\left(\frac{\partial G_{m-i-1}}{\partial x}\right)\right)\right)$$

$$+y(y-1)\frac{\partial^2 G_{m-1}}{\partial y \partial x} - \frac{x}{2}(y-1)\frac{\partial^2 G_{m-1}}{\partial x^2} - M^2 y\left(\frac{\partial G_{m-1}}{\partial x}\right) + \left(1 - M^2 y(1+E)\right)(1 - \chi_m),$$ (39)

$$R_m^\theta(\eta, \xi) = \frac{1}{m-1!}\frac{\partial^{m-1}N_\theta}{\partial q^{m-1}}\bigg|_{q=0} = \frac{1}{Pr}\left(\frac{\partial^2 \theta_{m-1}}{\partial x^2} + Nb\sum_{i=0}^{m-1}\frac{\partial \theta_{m-1-i}}{\partial x}\frac{\partial S_i}{\partial x} + Nt\sum_{i=0}^{m-1}\frac{\partial \theta_{m-1-i}}{\partial x}\frac{\partial \theta_i}{\partial x}\right)$$

$$+ y \sum_{i=0}^{m-1} G_i \frac{\partial \theta_{m-1-i}}{\partial x} + Ec \sum_{i=0}^{m-1} \frac{\partial^2 G_i}{\partial x^2} \frac{\partial^2 G_{m-1-i}}{\partial x^2} + y(y-1)\frac{\partial \theta_{m-1}}{\partial y} - \frac{x}{2}(y-1)\frac{\partial \theta_{m-1}}{\partial x} + \frac{4R}{3\Pr}\left[\frac{\partial^2 \theta_{m-1}}{\partial x^2} + (t_r - 1)^3\right.$$

,

$$\left(3\sum_{i=0}^{m-1}\left(\sum_{j=0}^{i}\theta_j\theta_{i-j}\sum_{k=0}^{m-1-i}\frac{\partial \theta_k}{\partial x}\frac{\partial \theta_{m-i-k-1}}{\partial x}\right) + \sum_{i=0}^{m-1}\left(\sum_{j=0}^{i}\theta_j\theta_{i-j}\sum_{k=0}^{m-1-i}\theta_k\frac{\partial^2 \theta_{m-i-k-1}}{\partial x^2}\right)\right) + 3(t_r - 1)\left(\sum_{i=0}^{m-1}\theta_i\frac{\partial^2 \theta_{m-1-i}}{\partial x^2}\right.$$

$$\left.+ \sum_{i=0}^{m-1}\frac{\partial \theta_i}{\partial x}\frac{\partial \theta_{m-1-i}}{\partial x}\right) + 3(t_r - 1)^2\left(\sum_{i=0}^{m-1}\sum_{j=0}^{i}\theta_j\theta_{i-j}\frac{\partial^2 \theta_{m-1-i}}{\partial x^2} + 2\left(\sum_{i=0}^{m-1}\sum_{j=0}^{i}\theta_j\frac{\partial \theta_{i-j}}{\partial x}\frac{\partial \theta_{m-1-i}}{\partial x}\right)\right)\right], \qquad (40)$$

$$R_m^S(x,y) = \frac{1}{m-1!}\frac{\partial^{m-1} N_S}{\partial q^{m-1}}\bigg|_{q=0} = \frac{\partial^2 S_{m-1}}{\partial x^2} + \frac{Nt}{Nb}\frac{\partial^2 \theta_{m-1}}{\partial x^2} + Sc\left[y\sum_{i=0}^{m-1} G_m \frac{\partial S_{m-1}}{\partial x} + y(y-1)\frac{\partial S_{m-1}}{\partial y}\right] - \frac{x}{2}(y-1)\frac{\partial S_{m-1}}{\partial x}$$

$$- y\omega S_{m-1}, \qquad (41)$$

where $G_m = \dfrac{1}{m!}\dfrac{\partial^m \xi_G(x,y,q)}{\partial q^m}\bigg|_{q=0}$, $\theta_m = \dfrac{1}{m!}\dfrac{\partial^m \xi_\theta(x,y,q)}{\partial q^m}\bigg|_{q=0}$ and $S_m = \dfrac{1}{m!}\dfrac{\partial^m \xi_S(x,y,q)}{\partial q^m}\bigg|_{q=0}$. $\qquad (42)$

The convergence of the following series of solutions is dependent on the appropriate choice of auxiliary parameters h_G, h_θ and h_S:

$$G(x,y,q) = G_0(x,y) + \sum_{m=1}^{\infty} G_m(x,y), \qquad (43)$$

$$\theta(x,y,q) = \theta_0(x,y) + \sum_{m=1}^{\infty} \theta_m(x,y), \qquad (44)$$

$$S(x,y,q) = S_0(x,y) + \sum_{m=1}^{\infty} S_m(x,y). \qquad (45)$$

To solve the above eqs., we have applied the symbolic software **Maple-18** and obtained the terms $G_m(x, y)$, $\theta_m(x, y)$ and $S_m(x, y)$ in the following form:

$$G_m(x, y) = c_1 + c_2 x + c_3 e^{-x} + G_{PS}, \tag{46}$$

$$\theta_m(x, y) = c_4 + c_5 e^{-x} + \theta_{PS}, \tag{47}$$

$$S_m(x, y) = c_6 + c_7 e^{-x} + S_{PS}, \tag{48}$$

where the suffix "PS" represents the particular solution. The all $c_i (i = 1..7)$ are calculated with the help of the boundary conditions (38).

4.1 Convergence of HAM solutions:

The convergences of series (43)-(45) are dependent on the appropriate values of auxiliary parameters h_G, h_θ and h_S which can be obtained by sketching h-curves[55]. We have sketched the h-curves with $G''(0, y)$, $\theta'(0, y)$ and $S'(0, y)$ for different values of y up to the 8th order of approximations and obtained a horizontal line in the ranges $h_G = [-0.048, 0]$, $h_\theta = [-0.048, 0]$ and $h_S = [-0.02, 0]$ which are displayed in **Fig.2**. **Table-1** represents the order of convergences of $G''(0, y)$, $\theta'(0, y)$ and $S'(0, y)$ for the values of auxiliary parameters, $h_G = -0.024$, $h_\theta = -0.012$ and $h_S = -0.004$ which indicates that the results are convergent up to four decimal places at 20th order of approximations. Hence, these are the appropriate values of auxiliary parameters h_G, h_θ and h_S. In **Table-2**, we present a comparison of the values of $\{-S'(0, y)\}$ obtained by homotopy analysis method and shooting method for steady non-radiative flow which presents a good agreement between both. **Table-3** shows the comparison of the present values of

$G''(0, y)$ with previous published values *i.e.* Wang[56] and Abbas *et al.* [57] for $M = 0$, $E = 0$, s = 0, $\lambda_1 = 0$ and different values of β. Excellent correlation is achieved confirming the validity of the HAM solutions.

5. DISCUSSION OF RESULTS

In this section, we present a brief discussion of influence of physical parameters on velocity $G'(x, y)$, temperature $\theta(x, y)$, concentration $S(x, y)$, skin friction coefficient Cf , local Nusselt number Nur, Sherwood number Shr and entropy generation number Ns via graphs and tables. The default values of leading parameters are taken as: $M = 0.1$, $E = 0.1$, $Nt = 0.1$, $Nb = 0.1$, $\Pr = 5$, $Ec = 0.3$, $R = 0.1$, $t_r = 1.5$, $\omega = 0.5$, $\beta = 0.1$, $s = 0.5$, $\lambda_1 = \lambda_2 = \lambda_3 = 2$, $Re = 1$, $\chi = 0.5$, $\Omega = 0.1$. The symbolic software Maple 18 running on personal computer (core i5) is used for finding HAM solution. The numerical HAM values of Nusselt number and Sherwood number are presented in **Table-4** with variation in the values of Ec, Nt, β, λ_2 & λ_3 and fixed values of other parameters. This table shows that these both quantities are decreased with an increase in the value of Eckert number and thermal slip parameter but increased with thermophoresis and stagnation parameter and also represents that Nusselt number increases as the values of mass slip parameter increases but Sherwood number decreases with an increase in the value of this parameter.

The profiles of velocity $G'(x, y)$, temperature $\theta(x, y)$ and concentration $S(x, y)$ in opposition to x are presented in **Fig 3** in which **Fig 3(a)** and **3(b)** are sketched to elucidate the effects of magnetic field parameter M and electric field parameter E on velocity. It is evident that $G'(x, y)$ is an increasing function of both of these parameters. The behavior of M can be

understood by the term $\dfrac{\sigma_{nf} B_0^2}{\rho_{nf}} (\bar{u} - \bar{u}_\infty)$ in the primitive momentum conservation eqn. (2). Since,

in our study, the boundary layer velocity $\bar{u}$ is less than the external free stream velocity $\bar{u}_\infty$,

therefore the term $\dfrac{\sigma_{nf} B_0^2}{\rho_{nf}} (u - u_\infty)$ become negative. Furthermore in the transformed momentum

conservation eqn. (8), the term $-M^2 y \left(\dfrac{\partial G}{\partial x} - 1 - E \right)$, both magnetic and electrical body force

terms become effectively positive. These body forces therefore assist momentum development

and lead to flow acceleration. Thus velocity increases with an increase in the value of magnetic

parameter, M. **Fig 3(c)** depicts temperature profile versus transformed transverse coordinate, x

for different values of radiation parameter R. It is apparent that $\theta(x, y)$ increases with an increase

in the value of R. This parameter is defined as $R = \dfrac{4\sigma_1 T_\infty^3}{k_{nf} k_1}$ and features in the augmented

thermal diffusion term in the heat conservation eqn. (9). It defines the relative contribution of

thermal radiation heat transfer to thermal conduction heat transfer. When $R < 1$ thermal

conduction dominates. When $R = 1$ both thermal conduction and thermal radiation contributions

are equal. For $R > 1$ thermal radiation dominates over thermal conduction. In the present

simulations, we confine attention to the last of these three cases i.e. $0 < R < 1$ wherein thermal

radiative flux is substantial. **Fig. 3 (c)** clearly reveals that there energizing of the flow with

increasing R values. This enhances thermal diffusion and therefore elevates temperatures and

also thermal boundary layer thickness. Similar observations have been reported by Shehzad *et al.*

[58] and Venkateswarlu *et al.* [27]. **Fig.3 (d)** depicts the concentration profile vs. x for different

values of chemical reaction parameter ω which shows that concentration is a decreasing function

of ω. We consider the destructive type of homogenous chemical reaction. Increasing the chemical reaction parameter ω produces a decrease in velocity and therefore also momentum boundary layer thickness is therefore increased substantially with greater chemical reaction effect. However concentration distributions decrease when the chemical reaction increases. Physically, for a destructive case, with stronger chemical reaction, greater destruction of the original nano-particle species takes place. This, in turn, suppresses molecular diffusion of the remaining species which leads to a fall in concentration magnitudes and a corresponding depletion in concentration boundary layer thickness.

Figs. 4(a) -4(c) illustrate the influence of magnetic parameter *M*, electric parameter *E*, Stefan blowing parameter *s*, dimensionless time τ, velocity slip parameter λ_1 and stagnation parameter β on skin friction coefficient *Cf*. *Cf* increases with an increase in the values of *M* since magnetic body force accelerates the flow whereas it decreases with electric field E. However the converse response is computed with *s*, λ_1 and β. In this figure, we have computed the effects of blowing parameter on skin friction for the values of $s = -1, 0, 1$. Here $s = -1$ indicates suction at the sheet surface, $s = 0$ implies a solid wall (no lateral mass flux) and $s = 1$ indicates injection at the wall. We have observed that as the value of blowing parameter (mass transfer) increases, skin friction at the surface decreases i.e. strong lateral mass flux into the boundary layer decreases the skin friction at the sheet surface.

Fig.5 depicts the combined effects of *s* and τ on local Nusselt number and Sherwood number; evidently both quantities are decreasing function of *s* but increasing function of τ. With greater progression of time therefore heat and mass transfer at the sheet (wall) is enhanced and wall

suction (s=-1) induces a similar influence. Wall injection (s=1) however depresses heat and mass transfer rates at the wall.

Fig.6 describes the effects of radiation parameter on *Nur* and *Shr* and shows that as the value of radiation parameter increases, the Nusselt number *increases* but Sherwood number *decreases*. Clearly with greater temperatures generated at higher values of radiation parameter the heat transferred to the wall is boosted. Conversely wall mass transfer rate is depressed owing to an increase in concentration of nano-particles in the boundary layer.

Fig. 7. shows that *Nur* and *Shr* are both increased with chemical reaction parameter. The destruction in nano-particle species with stronger chemical reaction effect (higher ω values), leads to a depletion in concentration values in the boundary layer. This encourages the transfer of species to the wall and elevates Sherwood number. The species diffusion to the wall also assist thermal diffusion and elevates wall heat transfer rates.

The second law of thermodynamics states that generally entropy of a system always increases. This statement is confirmed by **Fig 8 (a)-(c)** which depict the effects of magnetic parameter *M*, electric parameter *E* and Reynolds number *Re* on entropy generation number Ns. In all three graphs 8a-c, there is a non-trivial increase in entropy generation number Ns. Magnetic field, electrical field and inertial effect (Reynolds number) therefore all encourage entropy generation in the nanofluid regime. However **Fig. 8(d)** indicates that entropy generation number is decreased with an increment in chemical reaction parameter. When the temperature of any substance is minimized, this inhibits molecular motion and therefore the entropy of the system decreases.

Fig. 9(a)-(c). visualize the combined effects of parameters (M, E), (Nt, Nb) and (Re, R), in three-dimensional plots of Ns. Inspection of the **Fig.9(a)** reveals that Ns increases with an increase in the value of thermophoresis parameter Nt whereas the contrary behavior is generated with increasing Brownian motion parameter Nb. **Fig. 9(b)** shows the combined effects of Reynolds number and radiation parameter. With increasing Reynolds number, the entropy generation number also increases which is consistent with the results of **Fig. 8(c)**.There is a weak modification of Ns due to radiation parameter. Furthermore it is apparent that **Fig. 9(c)** concurs with the results of **Fig. 8(a)** and **8(b).**

6. CONCLUDING REMARKS

An analytical study of the collective influence of Stefan blowing and chemical reaction on unsteady nonlinear radiative EMHD stagnation-point flow of nanofluid from a stretching sheet has been presented with slip effects. Homotopy analysis method (HAM) solutions have been derived for the transformed, nonlinear partial differential boundary value problem. The principal conclusions of the present simulations may be summarized as:

- Velocity is an increasing function of magnetic and electric parameter. Temperature increases with an increase in the value of radiation parameter whereas concentration decreases with an increase in the value of chemical reaction parameter.

- Skin friction coefficient increases with an increase in the value of M and τ whereas it demonstrates the opposite response with s, β, E and λ_1. Local Nusselt number decreases with an increase in the value of Stefan blowing parameter s whereas it increases with R,

ω and τ. A similar response is computed for Sherwood number with s, ω and τ; however the converse trend is observed with R.

- Entropy generation number is an increasing function of M, E, Re, and Nt whereas it demonstrates the contrary behaviour with ω and Nb.

REFERENCES

1. Spalding DB. Mass transfer in laminar flow. *Proc R Soc Lond Ser Math Phys Sci* 1954; 221: 78–99.

2. Fang T and Jing W. Flow, heat and species transfer over a stretching plate considering coupled Stefan blowing effects from species transfer. *Commun Nonlinear Sci Numer Simul* 2014; 19: 3086–3097.

3. Uddin MJ Kabir MN and Bég OA. Computational investigation of Stefan blowing and multiple-slip effects on buoyancy-driven bioconvection nanofluid flow with microorganisms. *Int J Heat Mass Transf* 2016; 95: 116–130.

4. Uddin MJ Alginahi Y Bég OA and Kabir MN. Numerical solutions for gyrotactic bioconvection in nanofluid-saturated porous media with Stefan blowing and multiple slip effects. *Comput Math Appl* 2016; 72: 2562–2581.

5. Choi SUS and Eastman JA. Enhancing thermal conductivity of fluids with nanoparticles. Argonne National Lab., IL (United States); 1995. https://www.osti.gov/scitech/biblio/196525/ (accessed 28 Mar2017).

6. Buongiorno J. Convective Transport in Nanofluids. *ASME J Heat Transf* 2006; 128: 240–250.

7. Sheikholeslami M. Magnetohydrodynamic nanofluid forced convection in a porous lid driven cubic cavity using Lattice Boltzmann method. *J Mol Liq* 2017; 231: 555–565.

8. Sheikholeslami M. Influence of magnetic field on nanofluid free convection in an open porous cavity by means of Lattice Boltzmann method. *J Mol Liq* 2017; 234: 364–374.

9. Shahzad F Haq RU and Al-Mdallal QM. Water driven Cu nanoparticles between two concentric ducts with oscillatory pressure gradient. *J Mol Liq* 2016; 224: 322–332.

10. Sheikholeslami M and Bhatti MM. Active method for nanofluid heat transfer enhancement by means of EHD. *Int J Heat Mass Transf* 2017; 109: 115–122.

11 . Ul Haq R Noor NFM and Khan ZH. Numerical simulation of water based magnetite nanoparticles between two parallel disks. *Adv Powder Technol* 2016; 27: 1568–1575.

12 . Ul Haq R Hamouch Z Hussain ST and Mekkaoui T. MHD mixed convection flow along a vertically heated sheet. *Int J Hydrog Energy* 2017; 42: 15925–15932.

13 . Sheikholeslami M and Rokni HB. Melting heat transfer influence on nanofluid flow inside a cavity in existence of magnetic field. *Int J Heat Mass Transf* 2017; 114: 517–526.

14 . Sheikholeslami M and Sadoughi M. Mesoscopic method for MHD nanofluid flow inside a porous cavity considering various shapes of nanoparticles. *Int J Heat Mass Transf* 2017; 113: 106–114.

15 . Sheikholeslami M. Numerical simulation of magnetic nanofluid natural convection in porous media. *Phys Lett A* 2017; 381: 494–503.

16 . Sheikholeslami M and Rokni HB. Nanofluid two phase model analysis in existence of induced magnetic field. *Int J Heat Mass Transf* 2017; 107: 288–299.

17 . Sheikholeslami M and Zeeshan A. Analysis of flow and heat transfer in water based nanofluid due to magnetic field in a porous enclosure with constant heat flux using CVFEM. *Comput Methods Appl Mech Eng* 2017; 320: 68–81.

18 . Sheikholeslami M Gorji-Bandpy M and Ganji DD. Lattice Boltzmann method for MHD natural convection heat transfer using nanofluid. *Powder Technol* 2014; 254: 82–93.

19 . Khan U Ahmed N Mohyud-Din ST and Bin-Mohsin B. Nonlinear radiation effects on MHD flow of nanofluid over a nonlinearly stretching/shrinking wedge. *Neural Comput Appl* 2017; 28: 2041–2050.

20 . Bhatti MM and Rashidi MM. Effects of thermo-diffusion and thermal radiation on Williamson nanofluid over a porous shrinking/stretching sheet. *J Mol Liq* 2016; 221: 567–573.

21 . Sheikholeslami M. Magnetic field influence on nanofluid thermal radiation in a cavity with tilted elliptic inner cylinder. *J Mol Liq* 2017; 229: 137–147.

22 . Rashid I Ul Haq R and Al-Mdallal QM. Aligned magnetic field effects on water based metallic nanoparticles over a stretching sheet with PST and thermal radiation effects. *Phys E Low-Dimens Syst Nanostructures* 2017; 89: 33–42.

23 . Poornima T and Reddy NB. Radiation effects on MHD free convective boundary layer flow of nanofluids over a nonlinear stretching sheet. *Adv Appl Sci Res* 2016; 4.http://www.imedpub.com/abstract/radiation-effects-on-mhd-free-convective-boundary-layer-flow-of-nanofluidsrnover-a-nonlinear-stretching-sheet-14879.html (accessed 26 Aug2017).

24 . Mohyud-Din ST and Khan SI. Nonlinear radiation effects on squeezing flow of a Casson fluid between parallel disks. *Aerosp Sci Technol* 2016; 48: 186–192.

25 . Mishra SR Pattnaik PK Bhatti MM and Abbas T. Analysis of heat and mass transfer with MHD and chemical reaction effects on viscoelastic fluid over a stretching sheet. *Indian J Phys* 2017; 91: 1219–1227.

26 . Eid MR. Chemical reaction effect on MHD boundary-layer flow of two-phase nanofluid model over an exponentially stretching sheet with a heat generation. *J Mol Liq* 2016; 220: 718–725.

27 . Venkateswarlu B and Narayana PVS. Chemical reaction and radiation absorption effects on the flow and heat transfer of a nanofluid in a rotating system. *Appl Nanosci* 2015; 5: 351–360.

28 . Bég OA Ferdows M Bég ETA Ahmed T Wahiduzzaman M and M. Alam M. Numerical investigation of radiative optically-dense transient magnetized reactive transport phenomena with cross diffusion, dissipation and wall mass flux effects. *J Taiwan Inst Chem Eng* 2016; 66: 12–26.

29 . Matin MH and Pop I. Forced convection heat and mass transfer flow of a nanofluid through a porous channel with a first order chemical reaction on the wall. *Int Commun Heat Mass Transf* 2013; 46: 134–141.

30 . Kameswaran PK Narayana M Sibanda P and Murthy PVSN. Hydromagnetic nanofluid flow due to a stretching or shrinking sheet with viscous dissipation and chemical reaction effects. *Int J Heat Mass Transf* 2012; 55: 7587–7595.

31 . Ravi Kiran G Radhakrishnamacharya G and Bég OA. Peristaltic flow and hydrodynamic dispersion of a reactive micropolar fluid-simulation of chemical effects in the digestive process. *J Mech Med Biol* 2016; 17: 1–17.

32 . Ahmed S and Beg OA. Steady-state transport phenomena on induced magnetic field modeling for convective chemically reacting fluid with viscous dissipative heat. *Heat Transf Res* Published Online First: 30 September 2016.http://dx.doi.org/10.1615/HeatTransRes.2016008487 (accessed 26 Aug2017).

33 . Shukla N Rana P Beg OA and Singh B. Effect of chemical reaction and viscous dissipation on MHD nanofluid flow over a horizontal cylinder: Analytical solution. *AIP Conf Proc* 2017; 1802: 020015 (1-8).

34 . Bejan A. Method of entropy generation minimization, or modeling and optimization based on combined heat transfer and thermodynamics. *Rev Générale Therm* 1996; 35: 637–646.

35 . Tshehla MS and Makinde OD. Analysis of entropy generation in a variable viscosity fluid flow between two concentric pipes with a convective cooling at the surface. Published Online First: 2011.http://digitalknowledge.cput.ac.za/xmlui/handle/11189/2831 (accessed 26 Aug2017).

36 . Das S Chakraborty S Jana RN and Makinde OD. Entropy analysis of unsteady magneto-nanofluid flow past accelerating stretching sheet with convective boundary condition. *Appl Math Mech* 2015; 36: 1593–1610.

37 . Rehman S Haq R Khan ZH and Lee C. Entropy generation analysis for non-Newtonian nanofluid with zero normal flux of nanoparticles at the stretching surface. *J Taiwan Inst Chem Eng* 2016; 63: 226–235.

38 . Qing J Bhatti M Abbas M Rashidi M and Ali M. Entropy generation on MHD Casson nanofluid flow over a porous stretching/shrinking surface. *Entropy* 2016; 18: 1–14.

39 . Bhatti MM Abbas T and Rashidi MM. Entropy generation as a practical tool of optimisation for non-Newtonian nanofluid flow through a permeable stretching surface using SLM. *J Comput Des Eng* 2017; 4: 21–28.

40 . Abbas T Hayat T Ayub M Bhatti MM and Alsaedi A. Electromagnetohydrodynamic nanofluid flow past a porous Riga plate containing gyrotactic microorganism. *Neural Comput Appl* 2017; : 1–9.

41 . Liao SJ. *On the Proposed Homotopy Analysis Techniques for Nonlinear Problems and Its Applications*. 1992.http://www.scirp.org/(S(351jmbntvnsjt1aadkposzje))/reference/ReferencesPapers.aspx?ReferenceID=907769 (accessed 11 Apr2017).

42 . Liao SJ. *Beyond Perturbation: Introduction to the Homotopy Analysis Method*. Chapman & Hall/CRC Press, London/Boca Ratton; 2003. https://www.crcpress.com/Beyond-Perturbation-Introduction-to-the-Homotopy-Analysis-Method/Liao/p/book/9781584884071 (accessed 28 Jun2017).

43 . Liao S-J. On the analytic solution of magnetohydrodynamic flows of non-Newtonian fluids over a stretching sheet. *J Fluid Mech* 2003; 488: 189–212.

44 . Sajjad-ur-Rehman Rizwan-ul-Haq Lee C and Nadeem S. Numerical study of non-Newtonian fluid flow over an exponentially stretching surface: an optimal HAM validation. *J Braz Soc Mech Sci Eng* 2017; 39: 1589–1596.

45 . Gupta VG and Gupta S. Application of homotopy analysis method for solving nonlinear Cauchy problem. *Surv Math Its Appl* 2012; 7: 105–116.

46 . Ul Haq R Naveed Kazmi S and Mekkaoui T. Thermal management of water based SWCNTs enclosed in a partially heated trapezoidal cavity via FEM. *Int J Heat Mass Transf* 2017; 112: 972–982.

47 . Bhatti MM Abbas MA and Rashidi MM. A robust numerical method for solving stagnation point flow over a permeable shrinking sheet under the influence of MHD. *Appl Math Comput* 2018; 316: 381–389.

48 . Hsiao K-L. Stagnation electrical MHD nanofluid mixed convection with slip boundary on a stretching sheet. *Appl Therm Eng* 2016; 98: 850–861.

49 . Abdul Latiff NA Uddin MJ Bég OA and Ismail AI. Unsteady forced bioconvection slip flow of a micropolar nanofluid from a stretching/shrinking sheet. *Proc Inst Mech Eng Part N J Nanomater Nanoeng Nanosyst* 2016; 230: 177–187.

50 . Rajesh V Beg OA and Mallesh M. Transient nanofluid flow and heat transfer from a moving vertical cylinder in the presence of thermal radiation: Numerical study. *Proc Inst Mech Eng Part N J Nanomater Nanoeng Nanosyst* 2016; 230: 3–16.

51 . Abbas Z Hayat T Sajid M and Asghar S. Unsteady flow of a second grade fluid film over an unsteady stretching sheet. *Math Comput Model* 2008; 48: 518–526.

52 . Rana P Bhargava R and Bég OA. Finite element simulation of unsteady magneto-hydrodynamic transport phenomena on a stretching sheet in a rotating nanofluid. *Proc Inst Mech Eng Part N J Nanoeng Nanosyst* 2013; 227: 77–99.

53 . Hayat T Muhammad T Alsaedi A and Alhuthali MS. Magnetohydrodynamic three-dimensional flow of viscoelastic nanofluid in the presence of nonlinear thermal radiation. *J Magn Magn Mater* 2015; 385: 222–229.

54 . Bhatti M Abbas T Rashidi M and Ali M. Numerical Simulation of Entropy Generation with Thermal Radiation on MHD Carreau Nanofluid towards a Shrinking Sheet. *Entropy* 2016; 18: 200.

55 . Van Gorder RA and Vajravelu K. On the selection of auxiliary functions, operators, and convergence control parameters in the application of the Homotopy Analysis Method to nonlinear differential equations: A general approach. *Commun Nonlinear Sci Numer Simul* 2009; 14: 4078–4089.

56 . Wang CY. Stagnation flow towards a shrinking sheet. *Int J Non-Linear Mech* 2008; 43: 377–382.

57 . Abbas Z Sheikh M and Pop I. Stagnation-point flow of a hydromagnetic viscous fluid over stretching/shrinking sheet with generalized slip condition in the presence of homogeneous–heterogeneous reactions. *J Taiwan Inst Chem Eng* 2015; 55: 69–75.

58 . Shehzad SA Hayat T Alsaedi A and Obid MA. Nonlinear thermal radiation in three-dimensional flow of Jeffrey nanofluid: A model for solar energy. *Appl Math Comput* 2014; 248: 273–286.

Table-1 Order of Convergence of HAM results: Order of convergence of the values of $G''(0, y)$, $\{-\theta'(0, y)\}$ and $\{-S'(0, y)\}$ for the fixed values of parameters $\omega = 0.5, Nt = Nb = 0.1$, $Sc = 3$, $Ec = 0.5$, $M = 0.1$, $Pr = 5$, $E = 0.1$, $s = 0.5$, $R = 0.1$, $t_r = 1.5$, $\beta = 0.1$, $\lambda_1 = \lambda_2 = \lambda_3 = 5$, $y = 0.5$

Order	$G''(0, y)$	$\{-\theta'(0, y)\}$	$\{-S'(0, y)\}$
5	0.1498	0.1670	0.1668
10	0.1507	0.1672	0.1669
15	0.1509	0.1674	0.1669
20	0.1509	0.1674	0.1669
25	0.1509	0.1674	0.1669

Table-2 Validation of HAM Results: Comparison of HAM values of $\{-S'(0, y)\}$ with the values obtained by shooting method (limiting case) for the different values of Stefan blowing parameter s and fixed values of other parameters $Nt = Nb = 0.1$, $Sc = 5$, $Ec = 0.3$, $M = 0.1$, $Pr = 5$, $E = 0.1$, $R = 0$, $\beta = 0.1$, $\lambda_1 = \lambda_2 = \lambda_3 = 5$, $y = 1$, $\omega = 0.5$

s	$\{-S'(0, y)\}$	
	HAM	Shooting
0.1	0.1725	0.1726
0.3	0.1724	0.1724
0.5	0.1721	0.1723
0.7	0.1720	0.1721

Table-3: Comparison of present values of $G''(0, y)$ to the published results for particular case:

β	Present values	Wang [56]	Abbas *et al.*[51]
0	1.2327	1.232588	1.232587
0.1	1.1467	1.14656	1.146561
0.2	1.0511	1.05113	1.051129
0.5	0.7132	0.71330	0.713294
1	0	0	0

Table 4: HAM values of Nusselt and Sherwood number: The numerical values of Nusselt and Sherwood number obtained by homotopy analysis method on the fifteen order of approximations for the different values of *Ec*, *Nt*, β, λ_2 & λ_3 and fixed values of parameters *Nt* = *Nb* = 0.1, *Sc* = 10, M = 0.1, *Pr* = 5, *E* = 0.1, *R* = 0.1, $\lambda_1 = 3$, *y* = 0.5, $\omega = 0.5$.

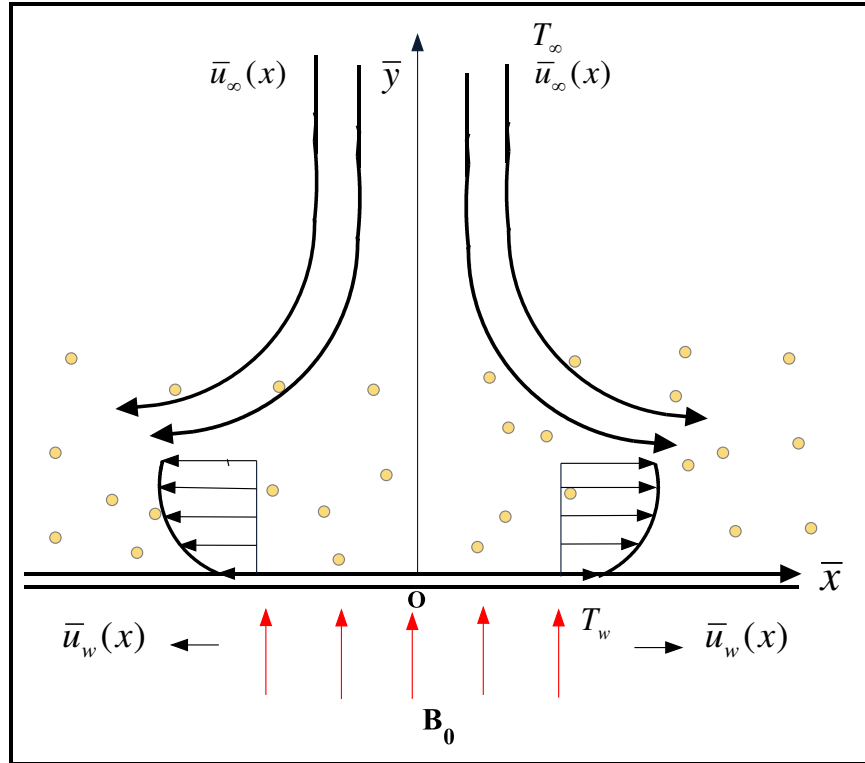|			(λ_2, λ_3)					
			(2, 2)		(2, 3)		(3,3)	
Ec	β	*Nt*	*Nur*	*Shr*	*Nur*	*Shr*	*Nur*	*Shr*
0.3	0.1	0.1	0.4915	0.6922	0.5008	0.5995	0.3670	0.5142
		0.25	0.5431	1.1939	0.5522	1.1033	0.4055	0.8902
		0.4	0.5947	1.6953	0.6036	1.6068	0.4439	1.2661
	0.1		0.4915	0.6922	0.5008	0.5995	0.3670	0.5142
	0.25	0.1	0.4919	0.6927	0.5012	0.5999	0.3673	0.5145
	0.4		0.4922	0.6933	0.5016	0.6003	0.3675	0.5149
0.5	0.1	0.1	0.4910	0.6919	0.5004	0.5992	0.3667	0.5140
		0.25	0.5426	1.1932	0.5518	1.1026	0.4051	0.8897
		0.4	0.5941	1.6942	0.6031	1.6057	0.4435	1.2653
	0.1		0.4910	0.6919	0.5004	0.5992	0.3667	0.5140
	0.25	0.1	0.4916	0.6925	0.5009	0.5997	0.3671	0.5144
	0.4		0.4920	0.6932	0.5014	0.6002	0.3674	0.5148

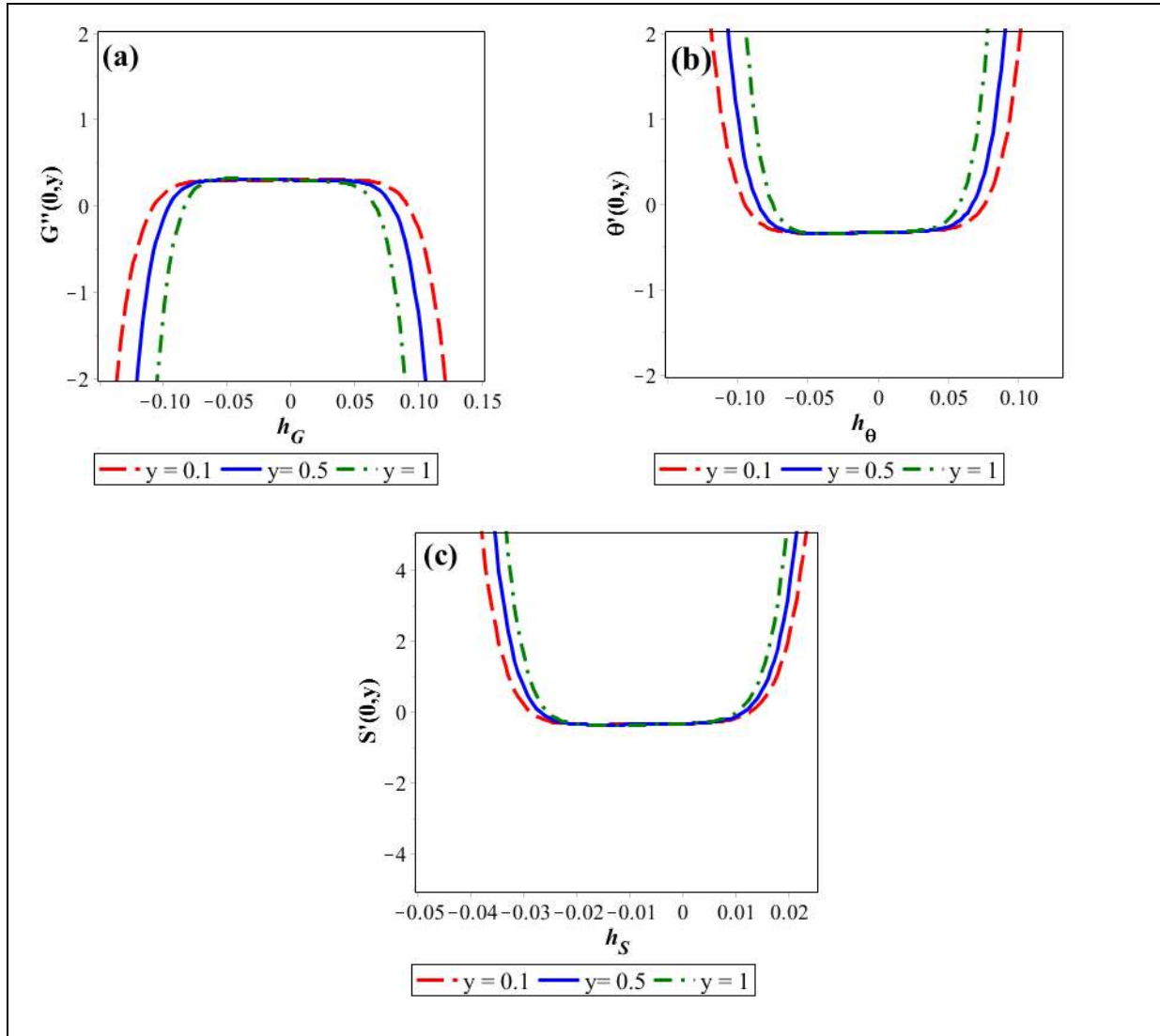**Fig.1** Physical structure of problem.

Fig.2 *h*-curve with $G''(0, y)$, $\theta'(0, y)$ and $S'(0, y)$ for different values of *y* on 8th order of approximations.
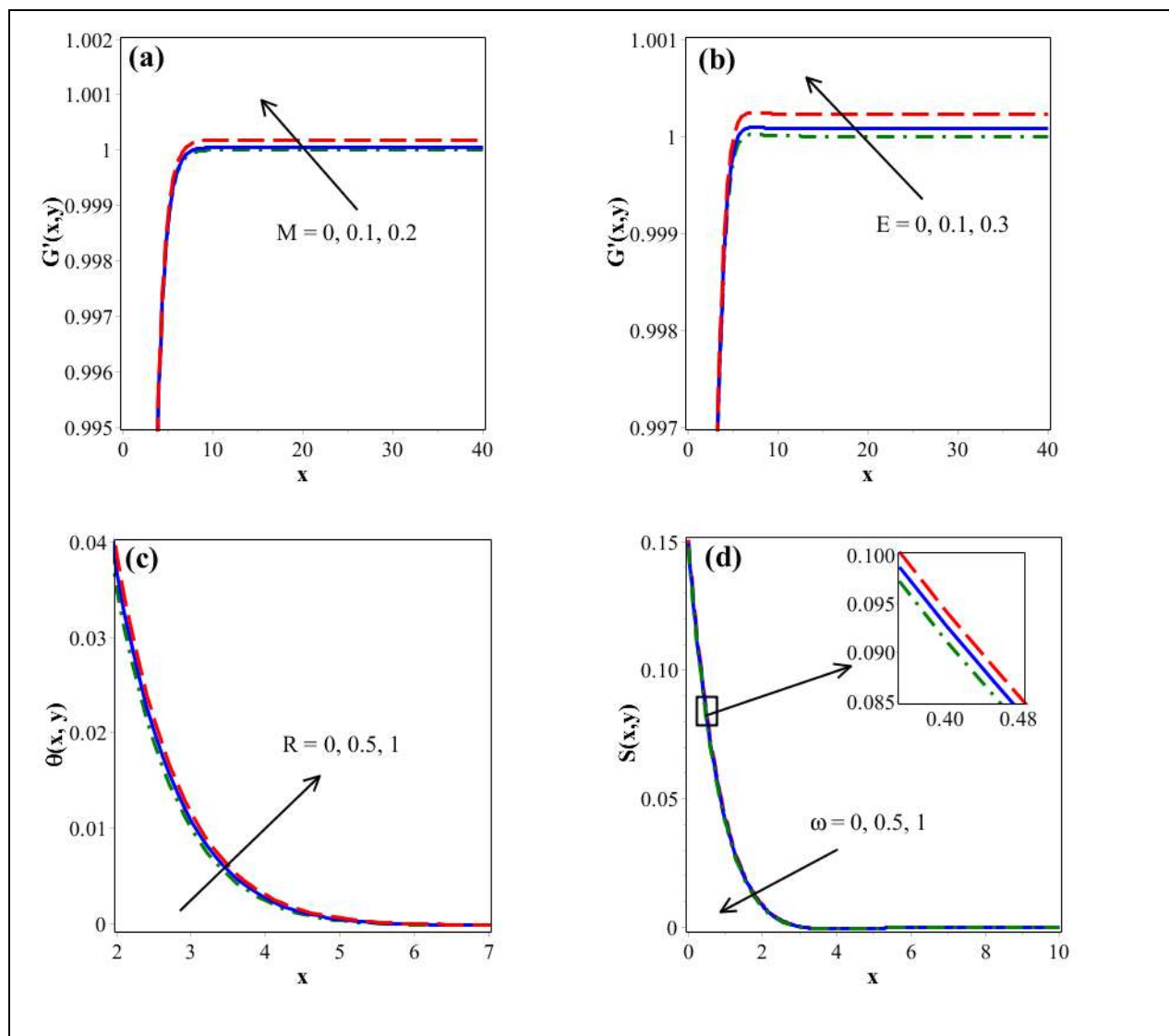
Fig.3 Effects of physical parameters on velocity $G'(x, y)$, temperature $\theta(x, y)$ and concentration $S(x, y)$.
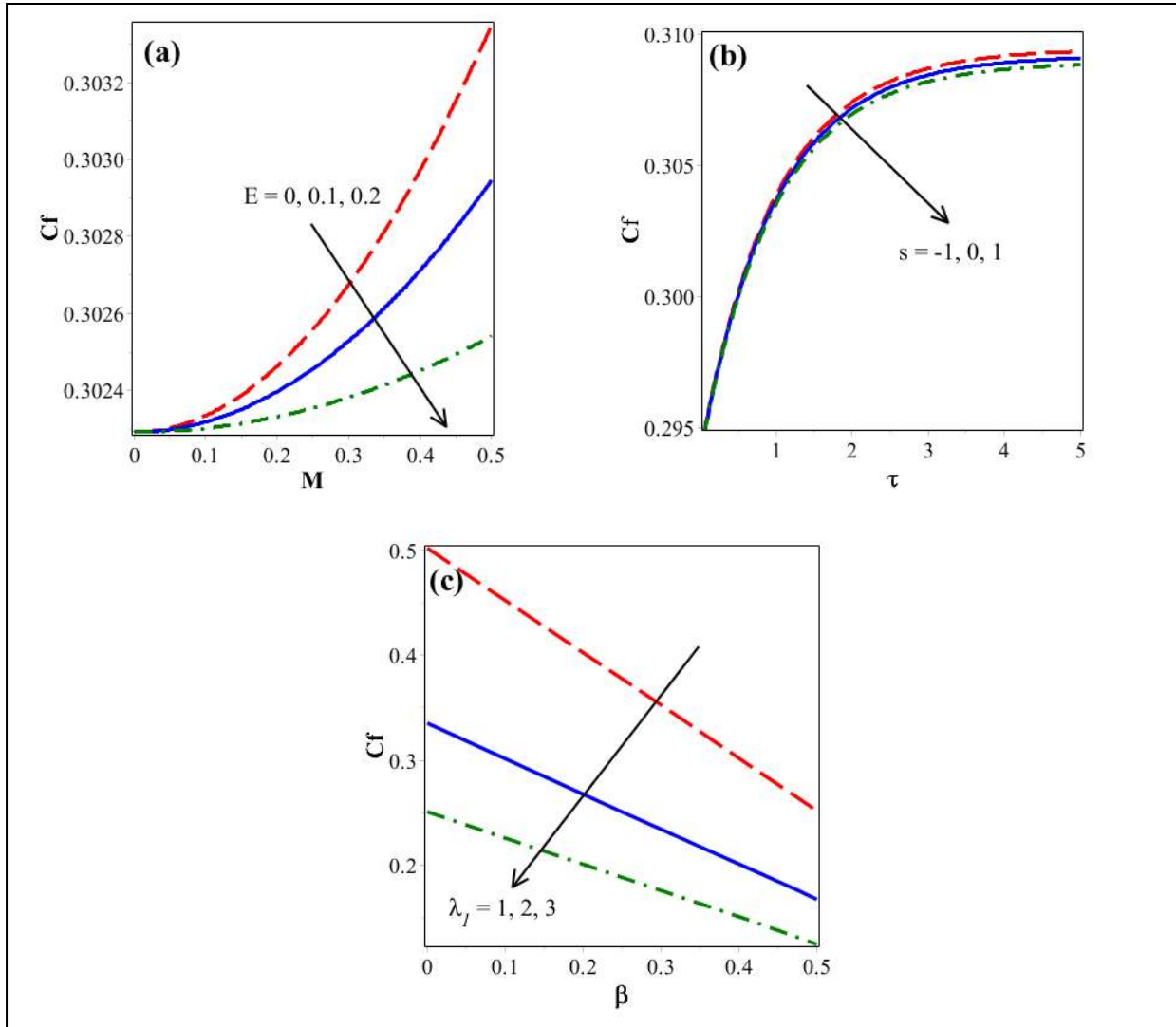
Fig.4 Combined effects of (E, M), (s, τ) and (λ_1, β) on skin friction coefficient.
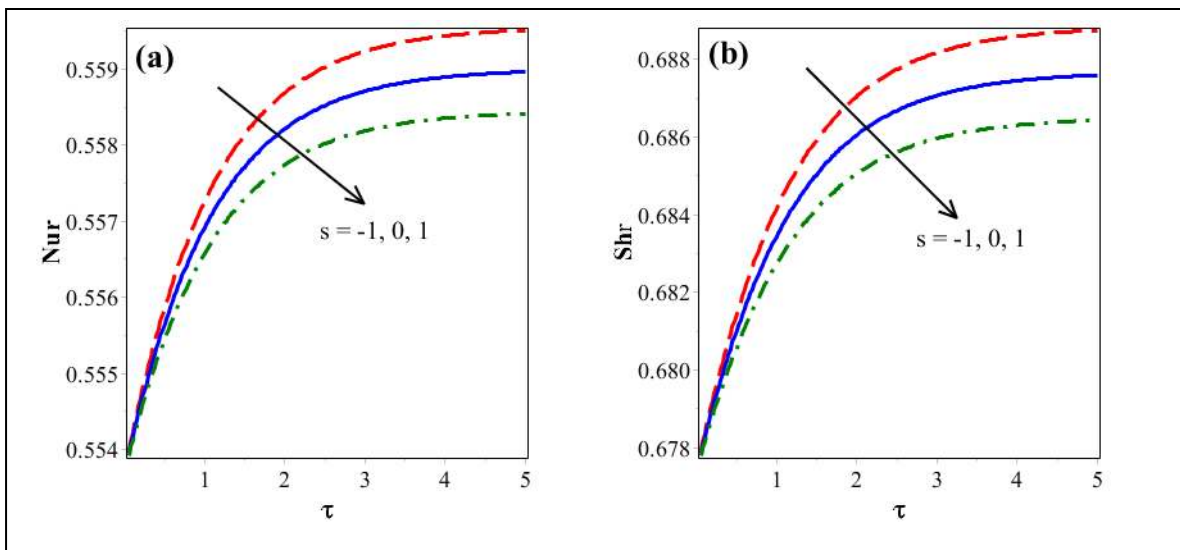
Fig. 5 Combined effect of *s* and τ on Nusselt and Sherwood number.
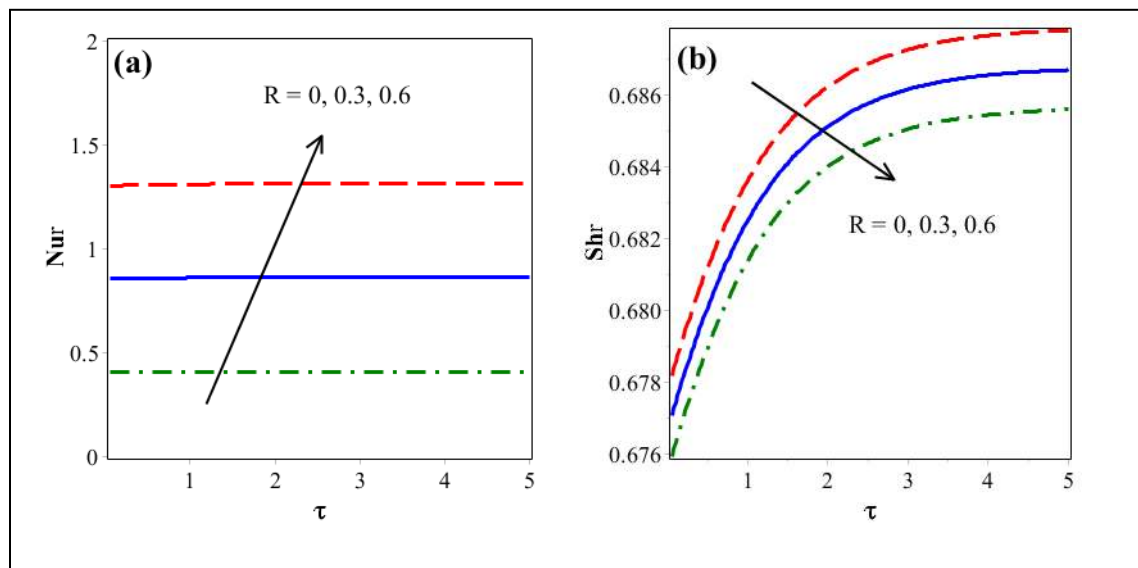
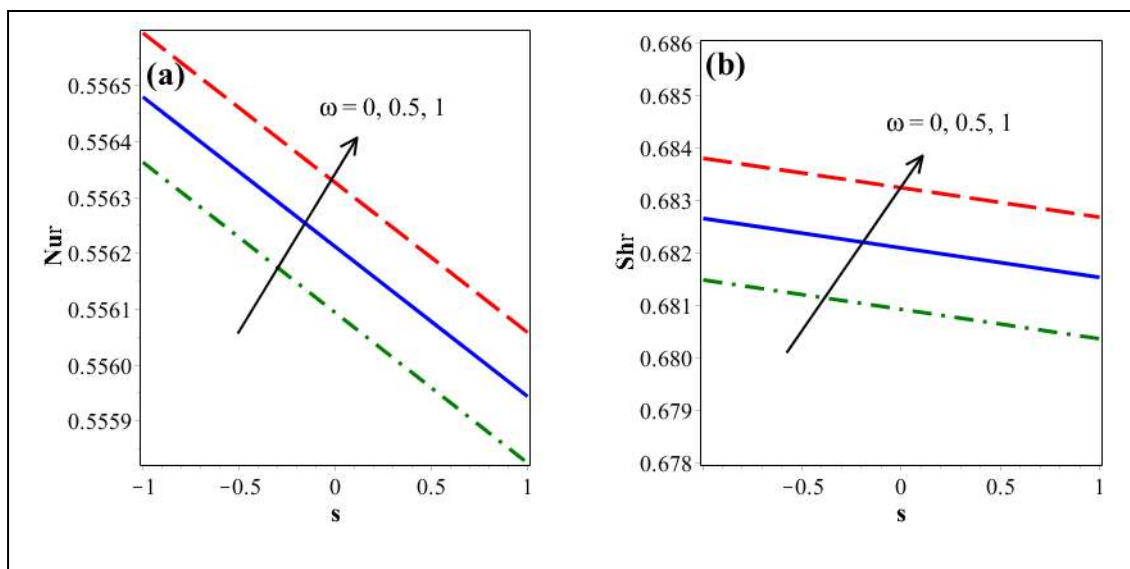**Fig.6** Combined effect of radiation parameter *R* and τ on Nusselt and Sherwood number.

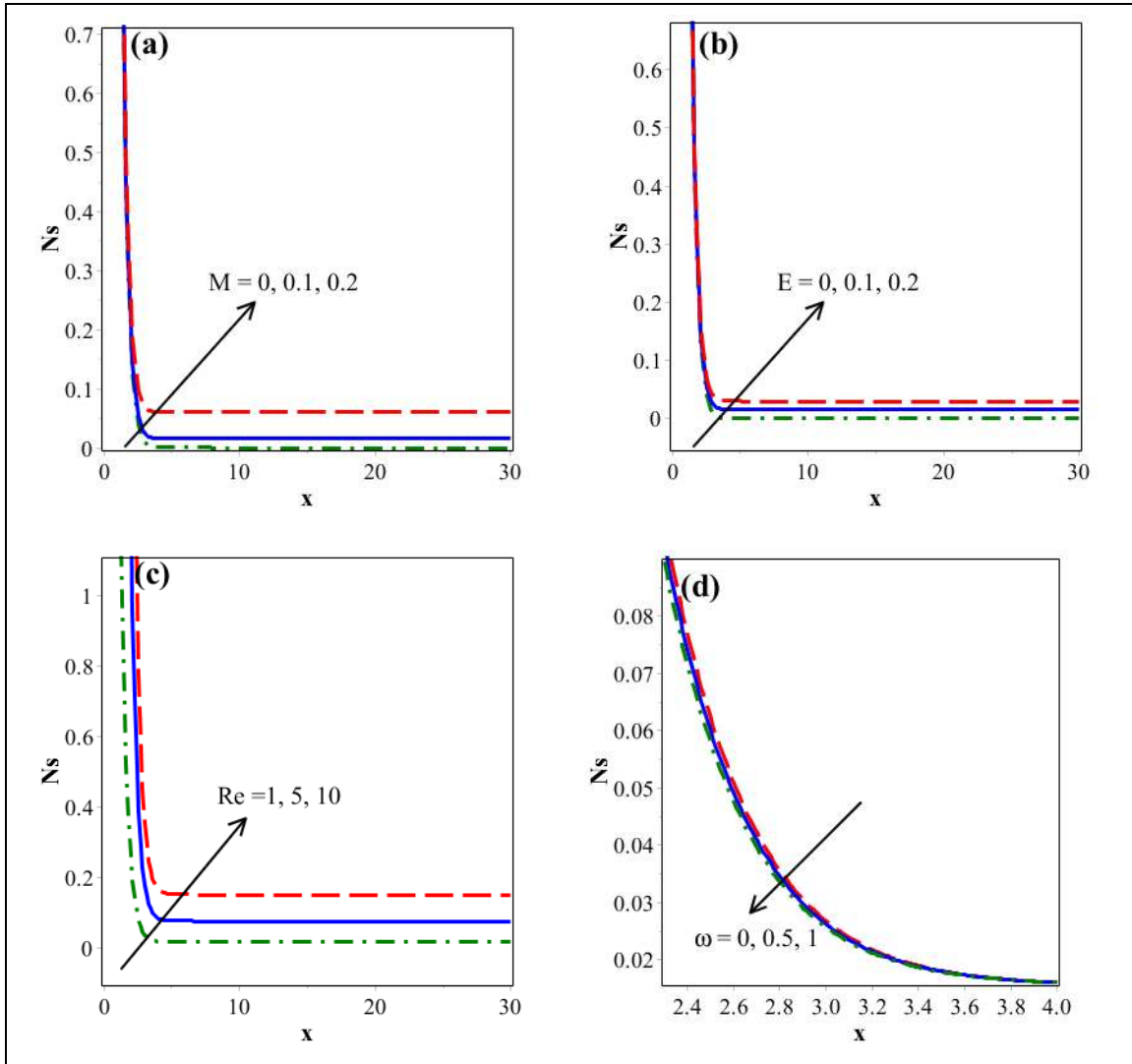**Fig. 7** Effect of chemical reaction parameter ω on Nusselt and Sherwood number.

Fig. 8 Effect of physical parameters *M*, *E*, *Re* and ω on entropy generation number *Ns*.
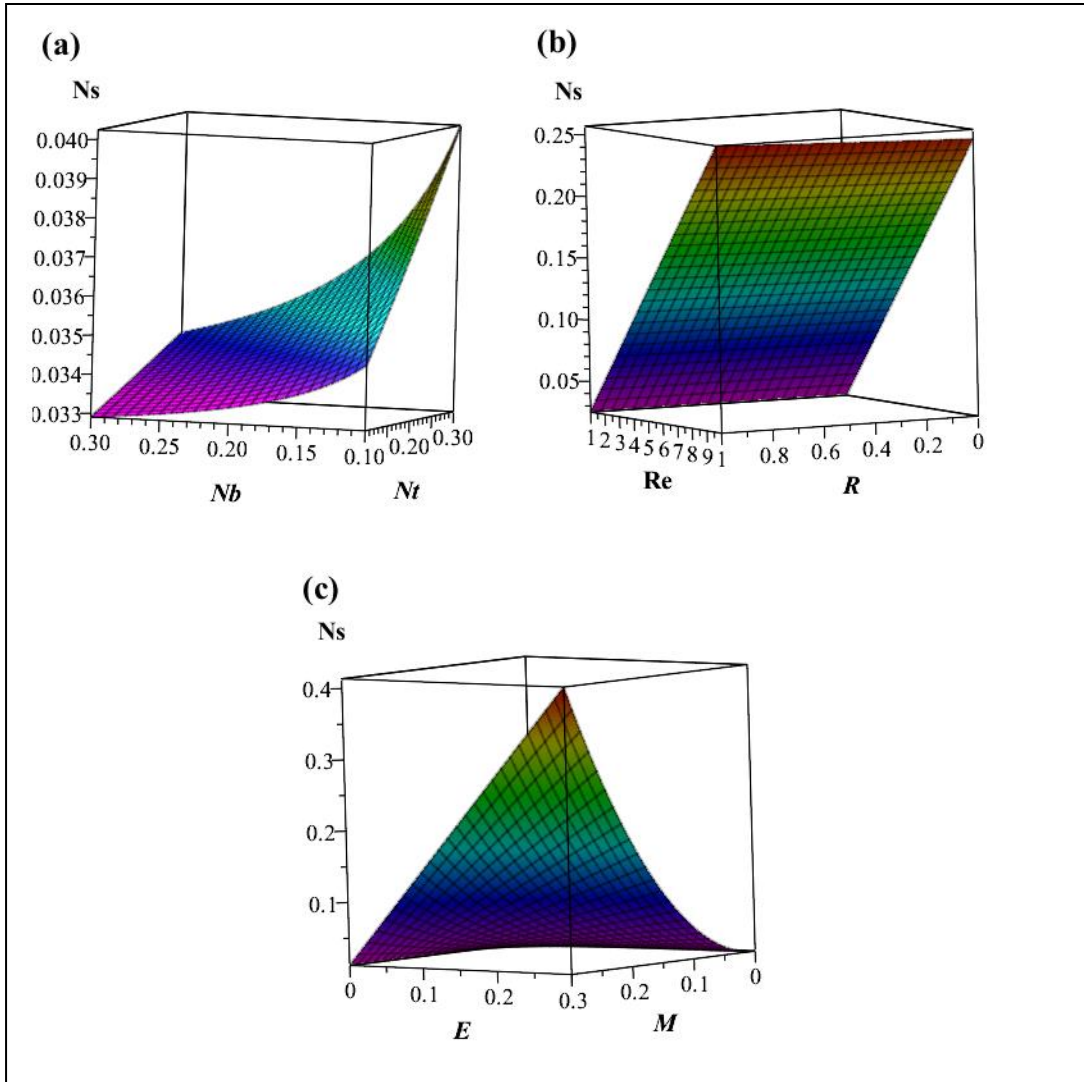
Fig.9 Combined effects of (*Nt*, *Nb*), (*Re*, *R*) and (*E, M*) on entropy generation number *Ns*.

List of Caption of Figures

Fig 1. Physical structure of problem.

Fig 2. *h*-curve with $G''(0, y)$, $\theta'(0, y)$ and $S'(0, y)$ for different values of y on 8th order of approximations.

Fig.3 Effects of physical parameters on velocity $G'(x, y)$, temperature $\theta(x, y)$ and concentration $S(x, y)$.

Fig.4 Combined effects of (E, M), (s, τ) and (λ_1, β) on skin friction coefficient.

Fig. 5 Combined effect of s and τ on Nusselt and Sherwood number.

Fig.6 Combined effect of radiation parameter R and τ on Nusselt and Sherwood number.

Fig. 7 Effect of chemical reaction parameter ω on Nusselt and Sherwood number.

Fig. 8 Effect of physical parameters M, E, Re and ω on entropy generation number Ns.

Fig.9 Combined effects of (Nt, Nb), (Re, R) and (E, M) on entropy generation number Ns.